Properties of Epitaxial Films Made of Relaxor Ferroelectrics

S. Prosandeev,[1,2] Dawei Wang,[3] and L. Bellaiche[1]

[1]*Physics Department and Institute for Nanoscience and Engineering, University of Arkansas, Fayetteville, Arkansas 72701, USA*
[2]*Physics Department and Institute of Physics, South Federal University, Rostov-on-Don 344090, Russia*
[3]*Electronic Materials Research Laboratory, Key Laboratory of the Ministry of Education and International Center for Dielectric Research, Xi'an Jiaotong University, Xi'an 710049, China*

(Received 11 August 2013; published 10 December 2013)

Finite-temperature properties of epitaxial films made of $Ba(Zr, Ti)O_3$ relaxor ferroelectrics are determined as a function of misfit strain, via the use of a first-principles-based effective Hamiltonian. These films are *macroscopically* paraelectric at any temperature, for any strain ranging between $\simeq -3\%$ and $\simeq +3\%$. However, original temperature-versus-misfit strain phase diagrams are obtained for the Burns temperature (T_b) and for the critical temperatures ($T_{m,z}$ and $T_{m,\mathrm{IP}}$) at which the out-of-plane and in-plane dielectric response peak, respectively, which allow the identification of three different regions. These latter differ from their evolution of T_b, $T_{m,z}$, and/or $T_{m,\mathrm{IP}}$ with strain, which are the fingerprints of a remarkable strain-induced *microscopic* change: each of these regions is associated with its own characteristic behavior of polar nanoregions at low temperature, such as strain-induced rotation or strain-driven elongation of their dipoles or even increase in the average size of the polar nanoregions when the strength of the strain grows.

DOI: 10.1103/PhysRevLett.111.247602 PACS numbers: 77.80.Jk, 77.55.D−, 77.55.Px, 77.80.bn

The need for miniaturized devices and the interest inherent to nanoscience have resulted in a vast amount of work devoted to epitaxial ferroelectric films in the last 20 years (see, e.g., Refs. [1–3] and references therein). In particular, the misfit strain arising from the difference in lattice constants between the material the film is made of and the substrate on top of which the film is grown has proven to be an effective tool to enhance properties and to generate novel phenomena. For instance, this strain can induce large piezoelectric, dielectric, and magnetoelectric responses in ferroelectric films [4–6], yield ferroelectric phases that are absent in a ferroelectric bulk [7–9], or even lead to the appearance of ferroelectricity in films made of systems that are paraelectric (or incipient ferroelectrics) in their bulk forms [10–14].

On the other hand, the influence of misfit strain on properties of an important and intriguing class of ferroelectrics is surprisingly still scarcely documented [15] and thus poorly known. This class is made of the so-called relaxor ferroelectrics, which are macroscopically paraelectric compounds that exhibit a frequency-dependent and broad dielectric response [16] and which have been intensively studied in their *bulk* forms for more than 60 years (see, e.g., Refs. [16–48] and references therein). This paucity of knowledge in films made of ferroelectric relaxors implies that many fundamental questions that are also pertinent to the development of novel technologies in different fields [49–51] remain unanswered. An example of such a question is the evolution of critical temperatures of relaxors (e.g., the Burns temperature [17] or the temperature at which the dielectric response is maximum) within a wide range of strains covering the compressive and tensile regimes. How the so-called polar nanoregions (PNRs), whose existence has often been advocated to be the microscopic origin of relaxor behaviors, respond to a misfit strain is also an open question. For instance, do the local electric dipoles inside the PNRs rotate when the misfit strain is varied around its zero, bulk value, as similar to the macroscopic polarization in classical ferroelectrics [7–9]? Do these PNRs become larger when the misfit strain adopts large values?

The goal of this Letter is to resolve all these issues by investigating epitaxial films made of $Ba(Zr, Ti)O_3$ (BZT) from first principles. Such solid solution was chosen because it is a known relaxor in its bulk form [52–60], and because PNRs were recently predicted to occur in BZT bulk [61]. As we will see, the present study allows us to reveal, and understand, how macroscopic and nanoscale properties depend on the misfit strain in epitaxial BZT films. In particular, it shows the existence of three different strain regimes, each having its own characteristic strain-induced evolution of dielectric and microscopic quantities.

Here, the first-principles-based effective Hamiltonian approach that has been developed in Ref. [61] is used to study epitaxial (001) BZT thin films having 50% of Ti and Zr compositions. These films are modeled by $12 \times 12 \times 12$ supercells that are periodic along the x, y, and z axes (which lie along the pseudocubic], [010], and [001] directions, respectively). We make use of an effective-Hamiltonian expansion for their internal energy, $E_{\mathrm{int}}(\{\mathbf{u}_i\}, \{\sigma_j\}, \{\mathbf{v}_i\}, \eta_H)$. $\mathbf{u}_i$ is the local soft mode in unit cell i, which is directly proportional to the local electric dipole moment in that cell. It is centered on the B sites (Zr or Ti) and represents the collective motion of Ba,

Zr/Ti, and oxygen atoms inside this cell. $\{\sigma_j\}$ characterizes the atomic arrangement, that is $\sigma_j = +1$ or -1 corresponds to the presence of a Zr or Ti atom located at the lattice site j, respectively, [62]. In the present study, the distribution of the Zr and Ti ions on the B sites of the supercell is chosen randomly and kept frozen, in order to simulate properties of *disordered* BZT compounds. Here, these properties are averaged (with the same weight) over 20 different realizations of such disordered supercells. The $\mathbf{v}_i$'s are Ba-centered dimensionless local displacements that are related to the inhomogeneous strain inside each cell [63]. η_H is the homogeneous strain tensor [63], and is relevant to mechanical boundary conditions. As a matter of fact, epitaxial (001) films are associated with the freezing of some components of η_H, namely (in Voigt notation) $\eta_{H,6} = 0$ and $\eta_{H,1} = \eta_{H,2} = \eta_{mf}$, with η_{mf} being the value forcing the film to adopt the in-plane lattice constant of the substrate [7,8,64]. The zero of misfit strain is chosen to correspond to the predicted lattice parameter of $Ba(Zr_{0.5}Ti_{0.5})O_3$ bulk at 130 K, that is 7.686 Bohr. Note that, as typically done in phenomenological or first-principle studies (see, e.g., Refs. [7,8]), only the strain experienced by the film is mimicked here. In other words, the effect of the film thickness on properties is not considered, since we use supercells that are periodic along any Cartesian direction. All the parameters entering the analytical expression of E_{int} are determined by performing first-principle calculations [65–67] on relatively small cells (namely, less than 20 atoms). Note that it was numerically found that the parameters quantifying the difference in ferroelectric strength between $BaZrO_3$ and $BaTiO_3$ (that is the difference between the harmonic coefficient being in front of the square of the polarization in a Landau-type phenomenology [68]) are crucial to explain relaxor behavior in BZT [61]. This is consistent with the fact that pure $BaZrO_3$ bulk is paraelectric [69], while pure $BaTiO_3$ bulk is ferroelectric. The E_{int} internal energy is then used inside Monte Carlo calculations having a relative large number of sweeps (namely, up to one million) to assure convergency of the results.

The misfit strain is allowed to vary between $\simeq -3\%$ and $\simeq +3\%$. For each elected η_{mf}, the system is progressively cooled down, starting from a high temperature of 2000 K. Figure 1 shows the diagonal components of the dielectric susceptibility tensor ($\chi_{\alpha\alpha}$, where $\alpha = x$, y, or z) as a function of temperature for four different misfit strains: a large compressive strain of -3.1% [panel (a)], a smaller compressive strain of -1.1% [panel (b)], a relatively small tensile strain of $+0.8\%$ [panel (c)], and a large tensile strain of $+2.8\%$ [panel (d)]. Note that $\chi_{\alpha\alpha}$ is computed by using the correlation function $\chi_{\alpha\alpha} = ((NZ^*)^2/V\varepsilon_0 k_B T)[\langle u_\alpha u_\alpha\rangle - \langle u_\alpha\rangle\langle u_\alpha\rangle]$ where $\langle u_\alpha u_\alpha\rangle$ denotes the statistical average of the square of the α component of the supercell average of the local mode vectors, and $\langle u_\alpha\rangle$ is the statistical average of that component. N is the number of the sites

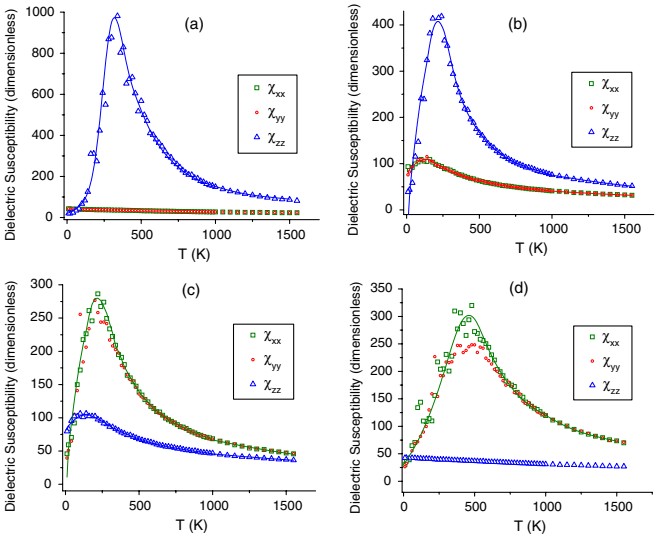

FIG. 1 (color online). Temperature dependency of the diagonal elements of the dielectric susceptibility, $\chi_{\alpha\alpha}$ (with $\alpha = x$, y, or z), of epitaxial films of $Ba(Zr_{0.5}Ti_{0.5})O_3$, for four different misfit strains. Panels (a), (b), (c), and (d) correspond to $\eta_{mf} = -3.1\%$, -1.1%, $+0.8\%$, and $+2.8\%$, respectively. The squares, circles, and triangles represent the numerical data for χ_{xx}, χ_{yy}, and χ_{zz}, respectively, while solid lines are guides for the eyes.

in the supercell, V is its volume, k_B is the Boltzmann constant, and ε_0 is the permittivity of the vacuum. T is the temperature and Z^* is the effective charge associated with the local mode [63].

Figure 1(a) indicates that, for large compressive strain, only χ_{zz} adopts a peak at a critical temperature, to be denoted as $T_{m,z}$, while χ_{xx} and χ_{yy} are equal to each other and relatively small for any temperature. The reverse situation holds for large tensile strain: the in-plane χ_{xx} and χ_{yy} susceptibilities possess a significant maximum at a finite critical temperature, to be referred to as $T_{m,\text{IP}}$, while the χ_{zz} out-of-plane susceptibility is small and slightly increases when decreasing the temperature [see Fig. 1(d)]. For intermediate values of the strains [cf. Figs. 1(b) and 1(c)], *both* the in-plane and out-of-plane susceptibilities have a peak, with the corresponding $T_{m,z}$ being larger (respectively, smaller) than $T_{m,\text{IP}}$ when the strain is compressive (respectively, tensile). The dielectric data of Fig. 1 thus already reveal a strong influence of the misfit strain on properties of films made of relaxors. What is also important to know is that all the epitaxial BZT films are found to be macroscopically paraelectric and cubic down to 0 K (i.e., the spontaneous polarization remains negligible down to the lowest temperatures), despite the existence of dielectric peak(s) for any investigated misfit strain. Such a feature is a well-known signature of ferroelectric relaxors [16]. We also found (not shown here) that the average magnitude of the Ti dipoles possesses a minimum at another (higher) critical temperature, to be denoted by T_b, for any misfit strain. We identify Tb as the so-called Burns temperature

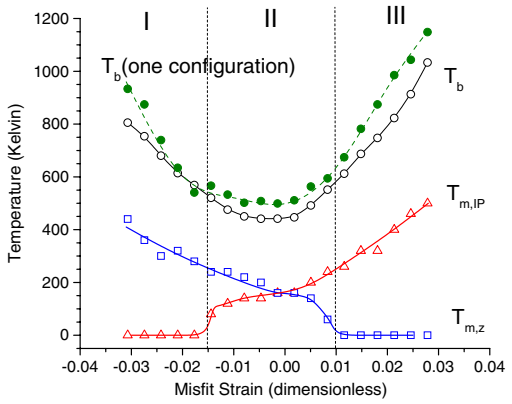

FIG. 2 (color online). Dependency of the critical temperatures on misfit strain, in epitaxial BZT films (as averaged over 20 different realizations of disorder). The open circles, triangles, and squares are numerical data for T_b, $T_{m,\mathrm{IP}}$, and $T_{m,z}$, respectively, while solid lines are guides for the eyes. The vertical dashed lines delimit the regions I, II, and III indicated in the text. The error bars on the numerical data are estimated to be around 50 K. The T_b temperatures associated with a single atomic configuration (which is chosen among the studied 20 realizations of disorder), is also shown by filled circles and a dashed line, to emphasize the effect of atomic distribution on physical properties of BZT systems and the need to average over different configurations to model complex disordered material.

[17]. Note that the T_b temperature in BZT bulk was recently determined to be associated with the formation of small Ti-rich clusters inside which the dipoles are parallel to each other [61].

Figure 2 displays the dependence of $T_{m,z}$, $T_{m,\mathrm{IP}}$, and T_b as a function of η_{mf}. The predicted Burns temperature is close to $\simeq 450$ K and only weakly depends on misfit strain when this latter ranges between $\simeq -1.5\%$ and $\simeq +1\%$. Such findings are consistent with the measured Burns temperature $\simeq 450$ K in $Ba(Zr_{0.5}Ti_{0.5})O_3$ *bulks* [53]. On the other hand, Figure 2 also shows that T_b significantly increases with the magnitude of the (compressive or tensile) strain, once this latter surpasses $\simeq 1.5\%$ in magnitude. For instance, the Burns temperature is as big as 1050 K for a tensile strain of around $+2.8\%$. We will provide an explanation for the dependence of T_b with strain later on. For now, let us turn our attention to the temperature-versus-misfit strain diagram arising from the dependence of $T_{m,z}$ and $T_{m,\mathrm{IP}}$ with η_{mf}. The phase diagram allows us to identify three different regions: region I that corresponds to compressive strains having a magnitude larger than $\simeq 1.5\%$, and for which there is no $T_{m,\mathrm{IP}}$ (i.e., the in-plane dielectric constant does not exhibit any peak down to 0 K) while $T_{m,z}$ significantly grows with the strength of the strain; region III that occurs for tensile strain being larger than $\simeq 1\%$, and for which it is $T_{m,z}$ that does not exist while it is $T_{m,\mathrm{IP}}$ that increases when the strain is increased; and, finally, region II that ranges between $\eta_{mf} = \simeq -1.5\%$ and $\eta_{mf} = \simeq +1\%$, and for which both $T_{m,\mathrm{IP}}$ and $T_{m,z}$ are finite with $T_{m,z}$ decreasing with strain while $T_{m,\mathrm{IP}}$ grows with η_{mf}. Strikingly, the overall shape of the phase diagram depicting $T_{m,z}$ and $T_{m,\mathrm{IP}}$ as a function of η_{mf} is remarkably similar to that of the temperature-versus-strain diagram of many "classical" ferroelectrics such as $BaTiO_3$ or $Pb(Zr, Ti)O_3$, once replacing regions I, II, and III by the so-called "c," "r," and "aa" phases [8,9,48,70,71]. However, an important distinction between the phase diagram of Fig. 2 and these latter temperature-versus-strain diagrams is that we did not find any macroscopic polarization in regions I, II, and III (unlike the cases of the "c," "r," and "aa" phases that are all ferroelectric and for which the polarization is along [001], [uuv], and [110] pseudo-cubic directions, respectively).

Such distinction strongly hints that some *microscopic*, short-range (rather than long-range) phenomenon is responsible for the evolution of $T_{m,z}$ and $T_{m,\mathrm{IP}}$ with η_{mf}. In order to find such a phenomenon, Fig. 3 displays the local dipole configurations in some (y, z) or (x, z) planes for three different strains, each associated with a specific region among regions I, II and III, at 10 K. For instance, Fig. 3(a) reports this configuration for a compressive $\eta_{mf} = -3.1\%$ and reveals that Ti clusters that have dipoles mostly oriented along either the *out-of-plane* [001] or [00$\bar{1}$] pseudo-cubic direction exist inside the BZT film in region I. As indicated by Fig. 3(c) that corresponds to a tensile strain of $+2.8\%$, these clusters still exist in region III, but their corresponding dipoles are now lying along the *in-plane* pseudocubic [110], [$\bar{1}$10], [1$\bar{1}$0], or [$\bar{1}\,\bar{1}\,0$] directions. Interestingly, in region II [cf. Fig. 3(b) for $\eta_{mf} = 0.2\%$], the dipoles align along the eight possible $\langle uuv\rangle$ directions inside Ti-rich clusters. We also numerically found (not shown here) that the magnitude of u is larger (respectively, smaller) than that of v if the epitaxial strain is tensile (respectively, compressive). In other words, the misfit strain induces a rotation of the electric dipoles inside the Ti-rich polar nanoregions (PNRs) of BZT films while the Zr-rich matrix remains paraelectric. Such rotation arises from the *local* coupling between strain and dipoles [7–9,48,63,64,72–74] but only inside the PNRs. Note that the PNRs (that are delimited by means of solid lines) in Fig. 3 were numerically found by Bayesian methods [75,76], as in Ref. [77].

To gain more information about the microscopic structure of BZT films, Figs. 4(a) and 4(b) display the dependence of two other quantities as a function of the misfit strain at 10 K. One quantity, shown in Fig. 4(a), is the average cluster size [78] that is defined as $\langle s\rangle = \langle N_{Ti}^2\rangle/\langle N_{Ti}\rangle$, where N_{Ti} is the number of Ti sites belonging to a PNR, and where "$\langle\cdots\rangle$" denotes the average over all the PNRs that are present in the supercell. Note that, practically, single-ion clusters are included in the computation of $\langle s\rangle$ while the so-called (infinite) percolating cluster is excluded [79]. The second quantity is indicated in Fig. 4(b), and is related to the averaged magnitude of the local dipoles centered on Ti and Zr sites,

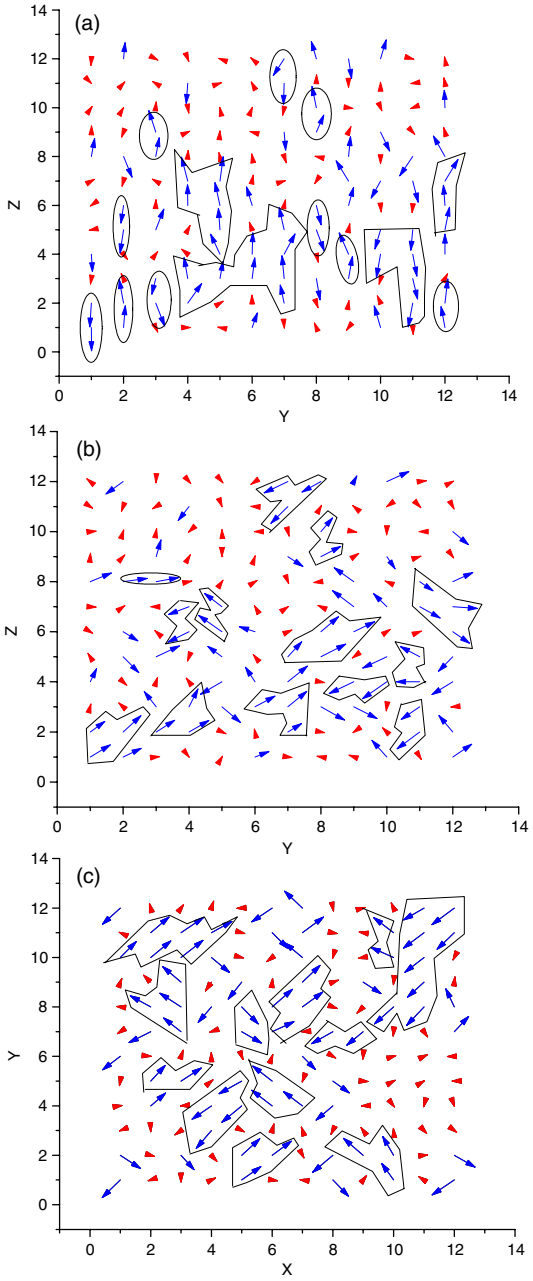

FIG. 3 (color online). Snapshots of the dipolar configurations in some planes for three different misfit strains, at 10 K. Panel (a) corresponds to a given (y, z) plane and $\eta_{mf} = -3.1\%$ (region I). Panel (b) also shows this (y, z) plane but for a strain of 0.2% (region II). Finally, Panel (c) is for a specific (x, y) plane and for a tensile strain of $+2.8\%$ (region III). Blue colors and red colors indicate that the corresponding local modes are centered on Ti and Zr ions, respectively.

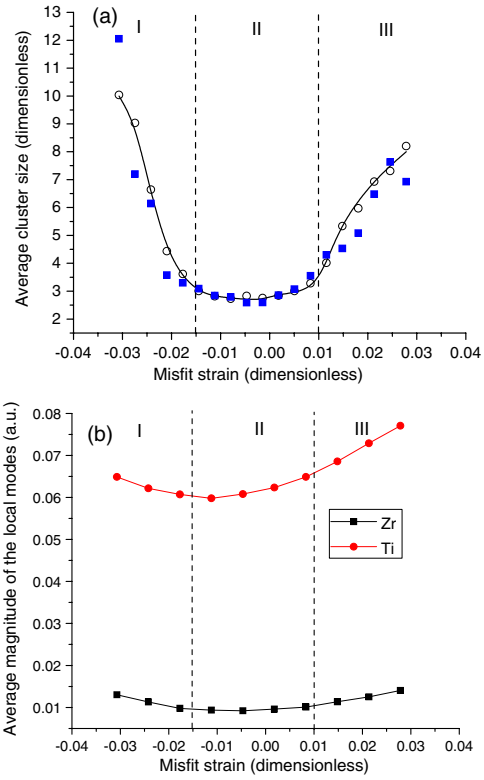

FIG. 4 (color online). Average cluster size (panel a) and average magnitude of the local modes centered on Ti and Zr ions (panel b) as a function of the misfit strain in epitaxial BZT films, at 10 K—as averaged over 20 different realizations of disorder. The vertical dashed lines delimit the regions I, II, and III indicated in the text. The average cluster size associated with a *single* atomic configuration is also displayed in panel a, by means of filled squares.

respectively. Figure 4, altogether with Fig. 3, are very informative to understand what is happening inside the BZT films as the misfit strain varies. As a matter of fact, Fig. 4 indicates that the average cluster size, as well as the magnitude of the local Ti and Zr dipoles, are basically unaffected by η_{mf} in region II. As a result, the predominant effect in this region, that is associated with relatively small magnitude of the strain, is the rotation of the dipoles inside Ti clusters as the strain varies. This "simple" rotation and, in particular, the strain insensitivity of $\langle s \rangle$ and of the average dipoles' magnitude also explains why the Burns temperature is basically independent of η_{mf} in region II (since the Burns temperature can be considered as the temperature at which PNRs begin to form [61], and since this formation should occur at larger temperature if the polar nanoregions are bigger and have larger dipoles at small temperature). On the other hand, region III is characterized by a significant increase of the average size of clusters (from $\simeq 3$ for $\eta_{mf} = +0.8\%$ to $\simeq 8$ for $\eta_{mf} = +2.8\%$) and an enhancement of the Ti dipoles along the $\langle 110 \rangle$ directions as the tensile strain increases. The morphology of the PNRs is therefore strongly modified by the strain. Figures 4(a) and 4(b) also indicate that the average cluster size also increases with the strength of the strain in the (compressive) region I, and that the Ti dipoles elongate more along the [001] or $[00\bar{1}]$ directions in the PNRs as the magnitude of η_{mf} grows in this region. Note that the rate of the growth of the PNRs (as calculated by computing $\langle s \rangle / \eta_{mf}$) is rather considerable, namely around 250 and -450 for

regions III and I, respectively, while the concomitant strain-induced change in the average magnitude of the Ti-centered dipoles is less significant in percentage [see Fig. 4(b)]. Interestingly, Fig. 4(b) further shows that the Zr dipoles also (slightly) increase with the strength of the misfit strain in regions I and III, therefore revealing that the matrix separating different PNRs begins to be polarized.

Let us also mention the role of atomic distribution on properties of BZT films. For that, Figs. 2 and 4(a) further show T_b and $\langle s \rangle$ for a single random configuration (that is chosen among the 20 used realizations of disorder). One can clearly see that these T_b and $\langle s \rangle$ can differ from those resulting from the average over the twenty different realizations of randomness, especially for a large magnitude of strain! Such a fact emphasizes the need to use several configurations when mimicking properties of disordered BZT systems. It can be understood by realizing that PNRs are Ti-rich regions, and that using different random configurations to assign the Ti locations automatically leads to different PNRs morphologies (and different interactions between them via the Zr-rich paraelectric matrix). Note also that the chemically ordered regions of $Pb(Sc_{0.5}Nb_{0.5})O_3$ (that were recently proposed to explain relaxor behavior in this system [80]) bear resemblance with our PNRs in BZT, in the sense that both of them do not possess random electric field. However, one difference between the two materials is that, outside these regions, BZT still does *not* possess any significant random electric fields while $Pb(Sc_{0.5}Nb_{0.5})O_3$ does. This is because the matrix is formed by *isovalent* Zr and Ti ions in BZT while it is formed by *heterovalent* Sc and Nb ions (that are disordered in the matrix) in $Pb(Sc_{0.5}Nb_{0.5})O_3$.

We hope that our study enhances the current fundamental knowledge of relaxor ferroelectrics and nanoscience. Research is supported by the Office of Naval Research, under Grants No. N00014-11-1-0384 and No. N00014-12-1-1034 (S. P., L. B.), by the U.S. Department of Energy, Office of Basic Energy Sciences, Division of Materials Sciences and Engineering under Award ER-46612 (D. W., L. B.). D. W. also acknowledges support from the National Natural Science Foundation of China under Grant No. 11104220. Some computations were made possible thanks to the MRI Grant No. 0722625, MRI-R2 Grant No. 0959124, and CI-TRAIN Grant No. 0918970 from NSF. S. P. appreciates Grant No. 12-02-92004 HHC-a of Russian Fund for Basic Research. The authors thank Dr. P.-E. Janolin and Dr. B. Dkhil for insightful discussions.

[1] M. Dawber, K. M. Rabe, and J. F. Scott, Rev. Mod. Phys. **77**, 1083 (2005).
[2] J. F. Scott, Science **246**, 1400 (1989).
[3] I. Kornev, H. Fu, and L. Bellaiche, J. Mater. Sci. **41**, 137 (2006).
[4] Z. Gui, S. Prosandeev, and L. Bellaiche, Phys. Rev. B **84**, 214112 (2011).
[5] S. Prosandeev, I. A. Kornev, and L. Bellaiche, Phys. Rev. B **83**, 020102 (2011) (R).
[6] J. C. Wojdel and J. Iñiguez, Phys. Rev. Lett. **105**, 037208 (2010).
[7] N. A. Pertsev, V. G. Kukhar, H. Kohlstedt, and R. Waser, Phys. Rev. B **67**, 054107 (2003).
[8] O. Dieguez, S. Tinte, A. Antons, C. Bungaro, J. B. Neaton, K. M. Rabe, and D. Vanderbilt, Phys. Rev. B **69**, 212101 (2004).
[9] B.-K. Lai, I. A. Kornev, L. Bellaiche, and G. J. Salamo, Appl. Phys. Lett. **86**, 132904 (2005).
[10] A. R. Akbarzadeh, L. Bellaiche, J. Íñiguez, and D. Vanderbilt, Appl. Phys. Lett. **90**, 242918 (2007).
[11] J. H. Lee *et al.*, Nature (London) **466**, 954 (2010).
[12] C. J. Fennie and K. M. Rabe, Phys. Rev. Lett. **97**, 267602 (2006).
[13] Y. Yang, W. Ren, D. Wang, and L. Bellaiche, Phys. Rev. Lett. **109**, 267602 (2012).
[14] J. H. Haeni *et al.*, Nature (London) **430**, 758 (2004).
[15] M. Tyunina, J. Levoska, P.-E. Janolin, and A. Dejneka, Phys. Rev. B **87**, 224107 (2013).
[16] L. E. Cross, Ferroelectrics **151**, 305 (1994).
[17] G. Burns and F. H. Dacol, Phys. Rev. B **28**, 2527 (1983).
[18] G. A. Smolensky *et al.*, *Ferroelectrics and Related Materials* (Gordon and Breach, New York, 1981).
[19] V. Westphal, W. Kleemann, and M. D. Glinchuk, Phys. Rev. Lett. **68**, 847 (1992).
[20] R. Pirc and R. Blinc, Phys. Rev. B **60**, 13 470 (1999).
[21] I.-K. Jeong, T. Darling, J. Lee, Th. Proffen, R. Heffner, J. Park, K. Hong, W. Dmowski, and T. Egami, Phys. Rev. Lett. **94**, 147602 (2005).
[22] Y. Bai and L. Jin, J. Phys. D **41**, 152008 (2008).
[23] H. Vogel, Phys. Z. **22**, 645 (1921).
[24] G. S. Fulcher, J. Am. Ceram. Soc. **8**, 339 (1925).
[25] B. Dkhil, P. Gemeiner, A. Al-Barakaty, L. Bellaiche, E. Dul'kin, E. Mojaev, and M. Roth, Phys. Rev. B **80**, 064103 (2009).
[26] O. Svitelskiy, D. La-Orauttapong, J. Toulouse, W. Chen, and Z. G. Ye, Phys. Rev. B **72**, 172106 (2005).
[27] S. Tinte, B. P. Burton, E. Cockayne, and U. V. Waghmare, Phys. Rev. Lett. **97**, 137601 (2006).
[28] V. M. Ishchuk, V. N. Baumer, and V. L. Sobolev, J. Phys. Condens. Matter **17**, L177 (2005).
[29] N. Takesue, Y. Fujii, M. Ichihara, and H. Chen, Phys. Rev. Lett. **82**, 3709 (1999).
[30] R. Blinc, A. Gregorovič, B. Zalar, R. Pirc, V. Laguta, and M. Glinchuk, Phys. Rev. B **63**, 024104 (2000).
[31] B. E. Vugmeister and H. Rabitz, Phys. Rev. B **57**, 7581 (1998).
[32] D. Viehland, S. J. Jang, L. E. Cross, and M. Wuttig, J. Appl. Phys. **68**, 2916 (1990).
[33] E. V. Colla, E. Y. Koroleva, N. M. Okuneva, and S. B. Vakhrushev, Phys. Rev. Lett. **74**, 1681 (1995).
[34] I. Grinberg, P. Juhas, P. K. Davies, and A. M. Rappe, Phys. Rev. Lett. **99**, 267603 (2007).
[35] A. Al-Zein, J. Hlinka, J. Rouquette, and B. Hehlen, Phys. Rev. Lett. **105**, 017601 (2010).
[36] Z. Kutnjak, C. Filipič, R. Pirc, A. Levstik, R. Farhi, and M. E. Marssi, Phys. Rev. B **59**, 294 (1999).

[37] A. Levstik, Z. Kutnjak, C. Filipic, and R. Pirc, Phys. Rev. B **57**, 11 204 (1998).

[38] A. A. Bokov and Z.-G. Ye, J. Adv. Dielect. **2**, 1241010 (2012).

[39] Z.-G. Ye and H. Schmid, Ferroelectrics **145**, 83 (1993).

[40] Z. Kutnjak, B. Vodopivec, and R. Blinc, Phys. Rev. B **77**, 054102 (2008).

[41] Z. Wu, W. Duan, Z. Liu, B.-L. Gu, and X. W. Zhang, Phys. Rev. B **65**, 174119 (2002).

[42] B. E. Vugmeister and H. Rabitz, Phys. Rev. B **65**, 024111 (2001).

[43] B. Dkhil and J. M. Kiat, J. Appl. Phys. **90**, 4676 (2001).

[44] R. Pirc, Z. Kutnjak, R. Blinc, and Q. M. Zhang, J. Appl. Phys. **110**, 074113 (2011).

[45] N. Novak, R. Pirc, M. Wencka, and Z. Kutnjak, Phys. Rev. Lett. **109**, 037601 (2012).

[46] I. P. Raevski, S. A. Prosandeev, A. S. Emelyanov, S. I. Raevskaya, E. V. Colla, D. Viehland, W. Kleemann, S. B. Vakhrushev, J.-L. Dellis, M. El Marssi, and L. Jastrabik, Phys. Rev. B **72**, 184104 (2005).

[47] R. Pirc, R. Blinc, and Z. Kutnjak, Phys. Rev. B **65**, 214101 (2002).

[48] A. Kvasov and A. K. Tagantsev, Phys. Rev. B **87**, 184101 (2013).

[49] C. Hofer, M. Hoffmann, U. Boettger, and R. Waser, Ferroelectrics **270**, 179 (2002).

[50] R. W. Whatmore and R. Watton, Ferroelectrics **236**, 259 (2000).

[51] C. B. Eom and S. Trolier-McKinstry, MRS Bull. **37**, 1007 (2012).

[52] R. Fahri, M. E. Marssi, A. Simon, and J. A. Ravez, Eur. Phys. J. B **9**, 599 (1999).

[53] T. Maiti, R. Gu, and A. S. Bhalla, J. Am. Ceram. Soc. **91**, 1769 (2008).

[54] R. L. L. Withers and B. Nguyen, Appl. Phys. Lett. **91**, 152907 (2007).

[55] A. Simon, J. Ravez, and M. Maglione, J. Phys. Condens. Matter **16**, 963 (2004).

[56] C. Laulhé, A. Pasturel, F. Hippert, and J. Kreisel, Phys. Rev. B **82**, 132102 (2010).

[57] A. Dixit, S. B. Majumder, R. S. Katiyar, and A. S. Bhalla, J. Mater. Sci. **41**, 87 (2006).

[58] A. A. Bokov, M. Maglione, and Z.-G. Ye, J. Phys. Condens. Matter **19**, 092001 (2007).

[59] V. V. Shvartsman, J. Zhai, and W. Kleemann, Ferroelectrics **379**, 77 (2009).

[60] D. Nuzhnyy, J. Petzelt, M. Savinov, T. Ostapchuk, V. Bovtun, M. Kempa, J. Hlinka, V. Buscaglia, M. T. Buscaglia, and P. Nanni, Phys. Rev. B **86**, 014106 (2012).

[61] A. R. Akbarzadeh, S. Prosandeev, E. J. Walter, A. Al-Barakaty, and L. Bellaiche, Phys. Rev. Lett. **108**, 257601 (2012).

[62] L. Bellaiche, A. García, and D. Vanderbilt, Phys. Rev. Lett. **84**, 5427 (2000); Ferroelectrics **266**, 41 (2002).

[63] W. Zhong, D. Vanderbilt, and K. M. Rabe, Phys. Rev. B **52**, 6301 (1995); Phys. Rev. Lett. **73**, 1861 (1994).

[64] I. Kornev, H. Fu, and L. Bellaiche, Phys. Rev. Lett. **93**, 196104 (2004).

[65] L. Bellaiche and D. Vanderbilt, Phys. Rev. B **61**, 7877 (2000).

[66] P. Hohenberg and W. Kohn, Phys. Rev. **136**, B864 (1964); W. Kohn and L. J. Sham, *ibid.* **140**, A1133 (1965).

[67] D. Vanderbilt, Phys. Rev. B **41**, 7892 (1990).

[68] L. D. Landau and E. M. Lifshitz, *Statistical Physics* Course of Theoretical Physics Vol. 5, Part 1 (Butterworth-Heinemann, London, 1980).

[69] A. R. Akbarzadeh, I. Kornev, C. Malibert, L. Bellaiche, and J. M. Kiat, Phys. Rev. B **72**, 205104 (2005).

[70] N. A. Pertsev, A. G. Zembilgotov, and A. K. Tagantsev, Phys. Rev. Lett. **80**, 1988 (1998).

[71] D. Sichuga, I. Ponomareva, and L. Bellaiche, Phys. Rev. B **80**, 134116 (2009).

[72] P. Ganesh and R. E. Cohen, J. Phys. Condens. Matter **21**, 064225 (2009).

[73] M. Ahart, M. Somayazulu, R. E. Cohen, P. Ganesh, P. Dera, H.-kwang Mao, R. J. Hemley, Y. Ren, P. Liermann, and Z. Wu, Nature (London) **451**, 545 (2008).

[74] Z. Wu and R. E. Cohen, Phys. Rev. Lett. **95**, 037601 (2005).

[75] E. T. Jaynes, *Probability Theory: The Logic of Science* (Cambridge University Press, Cambridge, England, 2003).

[76] Practically, the polar nanoregions are obtained using the following five-step process. (1) A Ti site (to be denoted as Ti_0) is selected and the direction of the dipole centered on that site is computed; (2) the dipoles centered on the Ti ions being first nearest neighbors of Ti_0 are investigated. If one of these dipoles (to be denoted as Ti_1) is similar in direction (within a pre-fixed angle criterion) with the dipole centered on Ti_0, then the site Ti_1 is added to the polar nanoregion (that already contains Ti_0); (3) an update of the average direction of the dipoles present in the polar nanoregion is then performed (using all the sites belonging so far to this nanoregion); (4) steps (2) and (3) are then repeated, but for Ti_1 rather than Ti_0, until no new sites can be added to the considered polar nanoregion; (5) one then starts from another Ti site that does not belong to any already determined polar nanoregion, and repeats steps (1)–(5) to obtain all polar nanoregions belonging to the supercell.

[77] S. Prosandeev, D. Wang, A. R. Akbarzadeh, B. Dkhil, and L. Bellaiche, Phys. Rev. Lett. **110**, 207601 (2013).

[78] D. Stauffer and A. Aharony, *Introduction to Percolation Theory* (Taylor & Francis, London, 1994).

[79] Note that, for the range of strain considered here, the phenomenon of percolation (i.e., the creation of an infinite cluster propagating through the entire system) is *not* systematically found for the 20 chosen different configurations—even at our largest investigated strain magnitude. This explains why the macroscopic polarization remains negligible down to the lowest temperatures for any studied strain.

[80] P. Ganesh, E. Cockayne, M. Ahart, R. E. Cohen, B. Burton, R. J. Hemley, Y. Ren, W. Yang, and Z.-G. Ye, Phys. Rev. B **81**, 144102 (2010).